First publ. in: Advanced Functional Materials 12 (2002), 3, pp. 197-202

Silica–Carbon Nanocomposites—A New Concept for the Design of Solar Absorbers**

By *Yitzhak Mastai*, *Sebastian Polarz*,* and *Markus Antonietti*

To create materials that are composites or hybrids structured on the nanometer scale or the meso-domain, respectively, is one of the major tasks in modern materials science. In this paper, we demonstrate general strategies on how to obtain these nanocomposites founded on the knowledge about ordered mesoporous materials. One strategy involves the formation of the composite by performing a chemical reaction in the pores of a pre-formed ordered mesoporous silica while the other strategy uses compounds that first mold their porous environment in the silica and in a succeeding step react to the final composite. As a model system, here, we present the formation of porous silica–carbon hybrid materials. Besides this more general question, we also tackle the task of finding a suitable application for the obtained nanocomposites. We chose an application as selective solar-absorber materials.

1. Introduction

Among the available energy resources, solar energy is considered to be an infinite and easy to handle energy available anywhere on the earth, and favorably in less developed countries, too. Furthermore, gaining energy from the sun is CO_2-neutral. Solar energy can be technically utilized in two ways. Light in the ultraviolet-visible (UV-vis) region is transferred to electric energy (solar cells), or radiation in the full spectral range is transferred to heat (solar absorbers). Obviously, transfer to heat has the potential to be an extremely efficient process.

The solar energy is commonly absorbed by a close-to-black surface with a strong absorption spectrum covering the whole range from the UV to the infrared (IR) with similar efficiency. While appropriate pigments and paints can establish appropriate solar absorption, a significant amount of solar energy or heat is re-emitted as IR rays by relaxation mechanisms within the material. These result in a reduced heat transfer from the absorbing surface to a suitable transport medium, such as water, therefore limiting the efficiency of such materials in photothermal applications.

It is therefore interesting to develop spectral selective solar absorbing materials that can be easily produced and processed. Selective absorber surfaces are characterized by high solar absorbance, α, (particularly in the UV-vis and near-IR regions) as well as by a low emissivity, ε, in the long wavelength (IR) region. An ideal selective absorber would be a material that absorbs all solar radiation without emission. For practical reasons, a selective absorber can be considered good if its total emissivity $\varepsilon \leq 0.20$ and absorbance $\alpha \geq 0.90$.

[*] Dr. S. Polarz, Dr. Y. Mastai, Prof. M. Antonietti
Max-Planck Institute of Colloids and Interfaces
Research Campus Golm
D-14424 Potsdam (Germany)
E-mail: polarz@mpikg-golm.mpg.de

[**] The Max-Planck Society is gratefully acknowledged for funding.

Selective absorber surfaces known so far are mostly cermet materials, namely, metal–dielectric composites.[1] The common design of selective solar absorbers is based on deposition of metallic particles in porous substrates, in which the porous substrate provides reflectance in the IR regions and the metallic particles provides the absorption in solar region. Nickel-pigmented alumina[2] is a classic example for such type of selective absorber system. Other systems designed in a similar manner with different metallic particles, e.g., Co,[3] Cr,[4] and in some cases with an additional antireflection layer to improve absorbance, are also known. Commercially available absorber materials show high solar absorbance ($\alpha \approx 0.96$) with low thermal emissivity ($\varepsilon \approx 0.12$) at temperatures ranging from ca. room temperature (RT), 20 °C, to 100 °C (293–373 K). However mass production of such materials is difficult and expensive. Moreover, the optical properties of those materials vary with time as a result of various degradation processes. Mainly oxidation of metallic particles at high temperature and humidity causes decreases of solar absorbance.[5] Furthermore, those materials are partially toxic, non-recyclable, and their unprotected exposure under conditions where leaching and oxidation is inevitable is at least environmentally questionable.

The search for alternative selective solar absorbers therefore has to consider a number of aspects. Firstly, the "spectral" properties have to be optimized, i.e., the materials should possess a high absorbance, but should be essentially IR-inactive. Secondly, the material has to be stable against heat, water, the exposure to heat-transfer solvents, and corrosive environments. Thirdly, the components of these materials have to be non-toxic, must be sufficiently cheap, and easy to produce.

In the current paper, we present a combination of porous silica[6–9] and nanosized carbon as a potential candidate for such a material. Silica is used as a transparent binder, whereas carbon nanoparticles are employed as the light-absorbing component. Both materials are easily available, non-toxic, stable against most external conditions, and do not leach out in any solvent. Both materials are essentially IR inactive, whereby carbon nanoparticles of sufficient size show a very strong absorption

over the whole UV-vis spectral range. As was said before, many metal-containing solar absorbers have been introduced[1–5,10–24] but using a "nano-carbon" containing material has not been reported to the best of our knowledge.

To prepare porous carbon–silica hybrid materials or nanocomposites, two general strategies exist, which are closely connected to the question of chemistry in porous media (Fig. 1).

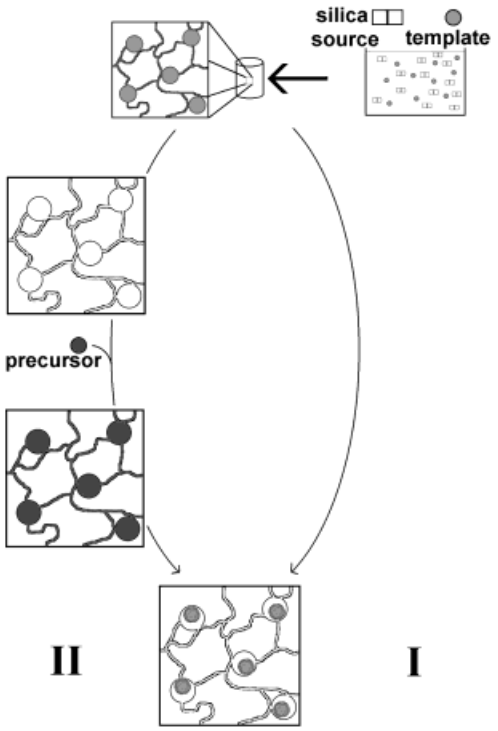

Fig. 1. Schematic presentation of the two routes (I and II) used to obtain porous carbon-containing silica materials via chemical transformation of suitable precursors in porous environments.

In route I, which was recently introduced,[25,26] appropriate carbon precursors are already used as porogens, i.e., a hybrid material of the silica precursor and the carbon precursor is cast (in the liquid state) and molded into the geometry of choice. By appropriate handling of the interface energies, such a mixture stays nanostructured, that is, both components demix only on the nanoscale, but are homogeneous on all larger scales. Heat treatment of this mixture under inert conditions (see Experimental part) results in an in-situ process in the desired cabon–silica nanocomposite. During this process the former porogen is transferred into the carbon nanoparticles, whereas the silica matrix acts as a confinement for the carbonization reaction.

In the second route, a porous silica material is made in a shape close to the one desired for final application. The porogen/template is removed to empty the pores, which are then filled with a carbon precursor. The precursor is transferred into elemental carbon in a carbonization reaction. (For a review on carbonization, see the literature.[27])

In the current paper we will present both strategies to prepare carbon–silica nanocomposites with different carbon cluster size. In both cases the reactors for the carbonization are restricted to nano-domain size using 1.5–3 nm thick SiO_2 walls to create compartments. Experiments are performed to see if these materials are suitable selective absorber materials.

2. Results and Discussion

Sugars are known to be good precursors for elemental carbon. Just by heating, dehydration occurs, which results in the formation of carbon. Together with the recent observation that cyclodextrins (CDs), cyclic oligo-saccharides containing 6, 7, or 8 sugar units, can be employed as templates for the formation of porous silica materials with a bicontinuous and "worm-type" pore system,[26,28] this results in the possibility of a one-step synthesis towards the desired carbon–silica nanocomposites by high-temperature treatment under non-oxidative conditions as monoliths or continuous coatings.

After carbonization (see Experimental part), the samples have been transformed from white or yellow transparent silica–sugar nanocomposites to deeply black, shining silica/carbon hybrids (see Fig. 2).

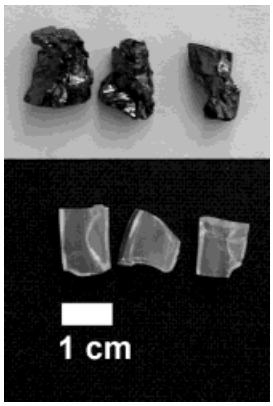

Fig. 2. Photographic image of porous silica monoliths before (lower images) and after carbonization (upper images).

According to elemental analysis, the carbon content of these samples after carbonization is 20 wt.-%; hydrogen is only present in insignificant amounts (≪1 %). From transmission electron microscopy (TEM), it is seen that the "worm-type" pore system typical for CD-based silicas (see Fig. 3a)[26,28] is conserved during carbonization, only the imaging-contrast be-

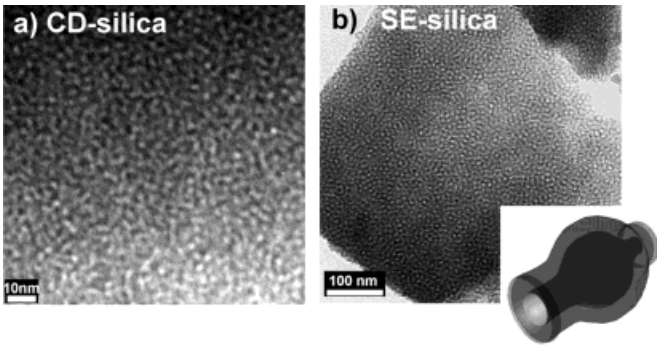

Fig. 3. TEM images of a typical CD-based porous silica (a), of SE1010-silica (b), and a schematic representation of the pore morphology of the SE1010-silica (inset).

tween the pores and the silica walls was lowered as compared to the empty CD-based silica (image not shown). The pores are now partially filled with carbon, which is hardly visible inside the porous silica in the TEM image. Sorption analysis delivered that the total surface area dramatically decreases due to pore blocking by carbon particles. The pure CD-based silica materials (no carbon inside) exhibit total surface values of about 800 $m^2 g^{-1}$ (Brunauer–Emmett–Teller, BET) while the carbon-containing samples have 300 $m^2 g^{-1}$. This value, however, still speaks for an open, porous structure, i.e., the water or other decomposition products had to leave the materials, and the voids were kept. Evaluation of the isotherms with a density functional theory (DFT) approach gives a pore size distribution very similar to the CD-based silica containing no carbon.

The silica matrix can be removed via HF etching, which allows to analyze the carbonization products separately. If done so, a black powder is obtained. Further analysis of this powder via TEM showed no "special" structure, which could be related to the silica, but rather aggregated carbon species far too large to be shaped by the pores. It has to be pointed out that TEM investigations on copper carbon grids make it nearly impossible to image 1.5 nm single carbon particles. Wide-angle X-ray scattering (WAXS) verifies that only amorphous carbon was formed (no graphite peaks). Just the agglomerates can be seen.

We also performed carbonization reactions in the SE1010-silica[29] (S = poly(styrene); E = poly(ethylene oxide); 10 = M_w = 1000 g mol^{-1}), which shows a comparable bicontinuous worm-type pore alignment (see Fig. 3b), but possessing larger mesopores with a diameter of 4.5 nm. As seen from gas sorption measurements, those worm-like pores are interconnected by smaller bottleneck channels.

Since we were not able to generate those larger channels with a carbonizable precursor, we employed the second route of carbon nanocomposite synthesis (see Fig. 1) by filling the mesoporous silica with the phenol–formaldehyde resin as an alternative carbon precursor.

The investigation of the carbon-containing SE1010-silica (see Fig. 4) leads to similar results as those for the CD-based silica. The carbon content is about 30 wt.-% here. The total surface area has decreased slightly through the incorporation of the carbon (from 633 $m^2 g^{-1}$ to 568 $m^2 g^{-1}$) but in this case the whole mesopore volume is still accessible, as seen by the isotherm (see Fig. 4).

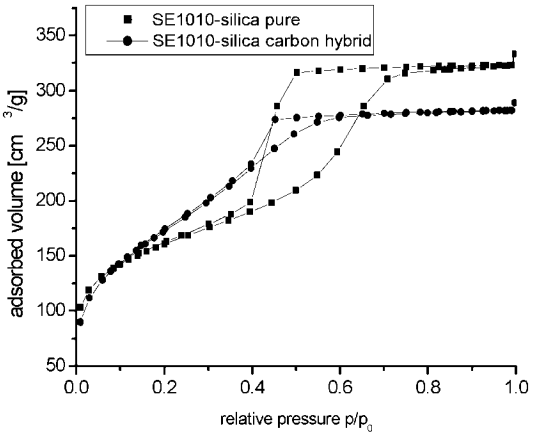

Fig. 4. Nitrogen sorption (T = –196 °C) isotherm for SE1010-silica with and without carbon.

Both isotherms of the pure and the carbon-containing silica are typical for mesoporous systems.[30,31] The mesopores are, as indicated by the very similar absolute surface area, not blocked, but just partly filled by the generated carbon. In addition, the hysteresis loop is narrowed, indicating a smoothing of the pore system and coverage of the silica wall with carbon. The calculated apparent pore diameter (determined by DFT analysis of the sorption data) of 4.5 nm for the pure SE1010-silica decreases slightly to 4 nm for the carbon containing analogue.

To characterize the structure of the carbon in the pores, the silica is again removed via HF etching. As a main product, a black powder is obtained, which consists of particle-like carbon. The single carbon particles have a similar shape and size to the original SE1010-silica pore or are smaller (see Fig. 5). A confinement or molding effect by the silica pores is probable but a direct correlation is difficult to deduce.

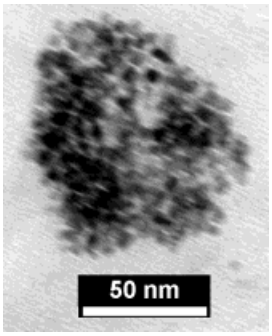

Fig. 5. TEM image of the carbon-phase resulting from carbonization in SE1010-silica.

The small particles with ca. 4.5 nm diameter agglomerate into larger aggregates, as is typical for strongly interacting carbon. WAXS reveals no graphite-like structure of these particles.

For an evaluation of the properties of the presented materials as selective solar absorbers their optical characteristics have to be investigated. Their solar absorbance, α_s, should be as close as possible to 1 (in the maximum of the solar spectrum) and they should have a minimum thermal emittance of radiation ε_T (≈0) in the IR region (λ > 2.5 μm).[32] For larger wavelengths the emission of radiation is not relevant because in this region the heat-transfer agent (e.g., water) begins to absorb the IR-radiation. Thus, the photothermal conversion efficiency η is defined as

$$\eta = \alpha_s - \varepsilon_T \quad (1)$$

The solar absorbance and the thermal emittance can be calculated from reflection measurments $R(\lambda)$ as follows

$$a_s = \frac{\int_{\lambda_1}^{\lambda_2} d\lambda [1 - R(\lambda)] P_{sun}(\lambda)}{\int_{\lambda_3}^{\lambda_4} d\lambda P_{sun}(\lambda)} \quad (2)$$

$$e_T = \frac{\int_{\lambda_4}^{\lambda_2} d\lambda[1-R(\lambda)]P_B(\lambda)}{\int_{\lambda_3}^{\lambda_2} d\lambda P_B(\lambda)} \quad (3)$$

where $P_{sun}(\lambda)$ the is sun-irradiation and $P_B(\lambda)$ is the spectral radiance of a black body at a temperature (T).[33] $P_B(\lambda)$ is therefore given by Planck's law (Eq. 4). Equation 3 describes the portion of the black-body radiation absorbed by the sample in relation to the total black-body radiation.

$$\frac{dP_B(\lambda)}{d\lambda} = \frac{2\pi hc^2}{\lambda^5}\frac{A}{\exp(\frac{hc}{kT}\lambda^{-1})-1}; \quad A = \text{surface area} \quad (4)$$

The optical properties of our materials in comparison with the two sources of energy exchange absorption of sun-radiation and emission via black-body radiation are given in Figure 6. The samples measured in diffuse reflection mode are marked with an "R". Emitting sources are denoted with "E".

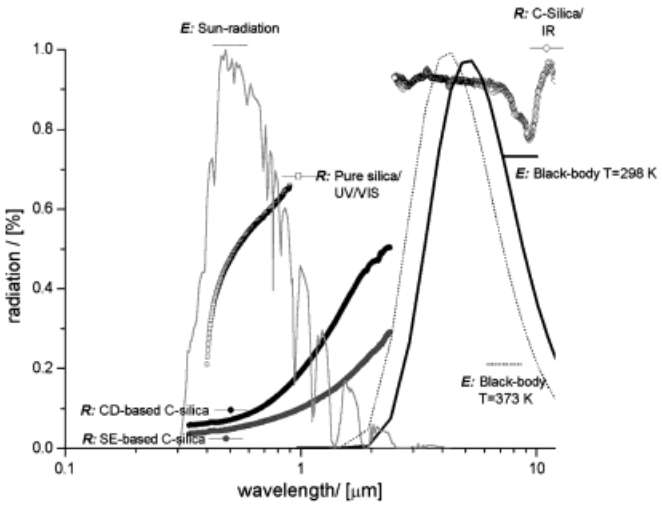

Fig. 6. Optical properties of the carbon–silica hybrid materials at different wavelengths (UV-vis/IR), determined by reflection measurements, in comparison to the sun-radiation that is absorbed and the energy emitted by black-body radiation at two temperatures. "R" denotes reflection measurements while "E" stands for sources of emission.

The pure SE-silica (without carbon) exhibits wide reflectance in the region of λ = 450–900 nm, as is typical for an opaque white or transparent object. The observed loss of intensity to 70–60 % reflectance is caused by scattering due to the powder-like morphology used for the measurement. Powders had to be used due to experimental reasons, and the reflectance of a monolith or film is certainly higher. Different from that, the diffuse reflectance is drastically reduced for the carbon-containing silica materials (the SE-based and CD-based materials are practically identical in this spectral region). For example, the diffuse reflectance of the carbon-containing SE-1010 silica at 600 nm is only 5 %, including powder scattering effects.

These findings can be quantified using the Equations 1, 2, and 3. Regarding the measurements, the solar absorbance, α_s, is 0.93 for the C-SE1010 silica and α_s = 0.92 for the C-CD silica.

When the samples are irradiated, four sources of energy leaving the sample can be identified: non-absorbed radiation, relaxation of the excited state by spectral emission, back-scattering from the materials surface, and black-body radiation. All these factors contribute to the total intensity in measurements of the total energy loss. In accordance to other reports the reflectance in the spectral region of 0.5–2.5 μm can be used to quantitatively decide which portion of the black-body radiation is released from the sample (Eq. 3).[32–34]

By treating the carbon particles inside the porous SiO_2 matrix as classical black-body radiators, ε_T can be estimated to be ε_T = 0.08 for the carbon-containing SE1010-based silica at T = 298 K. In the case of the CD-based material, the carbon particles are significantly smaller (diameter of ≈1.5 nm) and therefore exhibit a larger total surface area than the carbon particles resulting from the SE-silica. Due to that, the total energy loss by black-body radiation from the surface of the carbon particles has to be higher according to Planck's law (Eq. 4). This dependence is indeed seen, indicated by the higher values for the total reflectance (more energy is emitted from the sample) for the CD-based materials (see Fig. 6). Under this assumption the total emissivity is determined as ε_T = 0.13 (T = room temperature).

Therefore, the carbon/silica nanocomposites possess the required properties for selective solar absorbers. They highly absorb radiation in the solar region and do not show significant emission in the UV (they are black), but also in the IR region of the electromagnetic spectrum. From Equation 1, the photo thermal conversion efficiencies can be calculated as η = 0.85 for the carbon-containing SE-1010-silica materials and η = 0.79 for the carbon-containing CD-silica materials.

It must, however, be underlined that the data were determined on powders at normal incidence, whereas external shape of the sample or topography of the coating affect the photothermal conversion efficiencies of the final energy conversion device. Here, special surface topographies have to be chosen, such as the fly-eye geometry, which is possible, e.g., by microembossing of the solidifying sol–gel mixture.

Under the assumption that the absorptive properties do not change significantly with a change in temperature (which corresponds to other reports[32–34]) the efficiency of our materials decreases to $\eta_{SE\text{-}silica}$ = 0.82 and $\eta_{CD\text{-}silica}$ = 0.75 at T = 373 K (boiling point of water).

Since thermal instabilities and degradation of the solar active materials are the major disadvantages of the known metal particle containing selective solar absorbers, the stability of the carbon/silica nanocomposites was tested under relatively extreme conditions. Thermal stability tests of the samples were carried out in air. The samples were exposed to air for 48 h at different temperatures (200 °C, 250 °C, and 300 °C). Condensation tests, which simulate accelerated ageing of solar absorbers, were carried out according to the procedure reported by Wackelgard.[23] In brief, the samples are placed (exposure time 5 h) over a hot water bath at 100 °C, and the water vapor condenses on the sample surfaces. All samples exhibited thermal stability: the optical properties in the IR and UV-vis/near-IR region of the samples exposed to high temperatures (250–300 °C) in air

are identical to the as-prepared samples. Exposing the samples to water vapors leads to an additional broad band in the IR spectra (ca. 3300 cm^{-1}), typical for hydrated silica and assigned to water. Summarizing, the samples show good stability under influence of humidity and high temperatures. Even on longer time scales (3 days) the optical properties did not change at all. Bearing in mind the nature and the preparation conditions of our sample, namely high-temperature synthesis and the use of non-metallic absorbing particles, we can assume that the long-term stability of our samples is likely to be high. It should be emphasized that the lifetime of all thermal solar absorbers depends largely on the thermal oxidation of metal particles, a degradation that cannot occur in our samples.

3. Conclusion

We have shown that carbonization performed in the nano-confinements of porous silica can be used to prepare carbon–silica hybrid materials with light absorption properties. We have used both an in-situ approach where the porogens used to structure the silica are directly transferred to the carbon (controlled by the porous silica), as well as a loading technique where the porous silica is prepared first and is then loaded with a carbon precursor. The second technique, although clearly more complicated and demanding, has the advantage of a more flexible adjustment of the size and connectivity of the carbon structure.

The spectral behavior of the two materials, CD-based silica and SE1010-silica filled with amorphous carbon, were compared, and in both cases, high photo-thermal conversion efficiencies were found. Nevertheless, the SE1010 based silica with its 4.5 nm large carbon chromophores turned out to be still a little more efficient than the CD-based silica with its smaller carbon nanostructures. This points to the fact that further engineering of the carbon structure might result in a further improvement of the efficiency.

The resulting products are true hybrid materials or nanocomposites containing SiO_2 and carbon in a rational designed way, they are not just physical mixtures of both components (see Fig. 7). The carbon nanoparticles contribute the very high absorbance and thermal/chemical stability, wheras silica contributes the transparency, processability, binding, and coating properties.

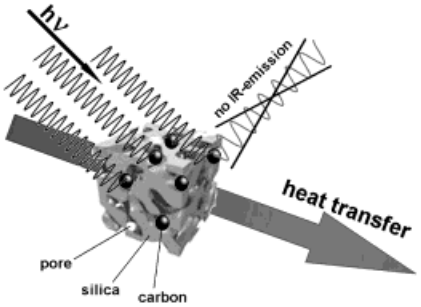

Fig. 7. Schematic representation of the obtained materials. Direct carbonization in porous silica materials leads to the formation of nano-sized carbon particles confined by the pore walls. Electromagnetic radiation is absorbed and, without re-emission in the IR-region, transferred into kinetic energy (heat). Due to the porosities of the materials this heat can be removed by infiltration with heat-transfer solvents of any kind (preferentially water) without any degradation of the material.

As compared to a bare mixture of carbon and silica, the nanocomposite gains some advantages originating from the structural architecture on a nano-scale. These advantages are the low internal scattering, the possible spectral adjustment of the carbon chromophore, the high mechanical performance of a nanocomposite, as well as an optimized heat transfer between the carbon and silica subphase and a potential additional heat transfer agent, which can be filled in the pores.

Especially in the CD case, the overall process is ideal for the preparation of carbon–silica nanocomposites under "green-chemistry" conditions. The carbon precursor itself is chemically a sugar, easily available, and non-toxic. The carbon–silica hybrids are obtained under one-pot conditions with the elimination of water only; no removal or addition of any further chemical is necessary to obtain the non-toxic carbon-containing silicas. In addition, leaching of the final material is practically impossible and would result only in the release of a product already abundant in nature.

4. Experimental

Materials: CD derivatives that are employed as porogens and carbon precursor were obtained from the Wacker AG/Germany. In addition, the phenol–formaldehyde precursor A203 from Huntsman was used for carbonization. All other chemicals were obtained from Aldrich and used without further purification. The preparation and characterization of the corresponding silica materials was already reported before [28,29] and will only be briefly described.

Sample Preparation: The CD-containing silicas are prepared as follows: 2 g β-methylated CD (β-MCD) are dissolved in 3 g of aqueous HCl (pH 2) and 4 g tetramethylorthosilane (TMOS) are added. Homogenization occurs in a few minutes. The evolving methanol is removed in vacuum and the resulting gels are aged for 48 h at 60 °C [28]. Under these conditions the CD-molecule is absolutely stable.

The SE1010-silica was prepared according to the procedure published by Göltner et al. [29]. 1 g block copolymer SE1010 (S = poly(styrene); E = poly(ethylene oxide); 10 = M_w = 1000 g mol^{-1}) is dissolved in 2 g of TMOS. Then 1 g of aqueous HCl (pH 2) is added. After homogenization, the methanol is removed in vacuum. The resulting gels are aged for 24 h at 60 °C. The SE1010-template is removed via calcination in air at 550 °C for 5 h in a tube oven.

To load the porous silica with a carbon precursor, 3 g of the phenol–formaldehyde resin A203 are dissolved in 4 g of acetone. 3 g of the calcined, porous SE1010-silica are impregnated with the carbon precursor solution for 24 h. The resulting dispersion is filtrated under suction and dried at RT, resulting in pale yellow fragments of loaded silica.

The carbonization experiments were performed as follows. No addition of a carbon precursor is necessary for CD-containing silica, as the CD is transformed in situ into carbon. The samples are heated in a tube oven to 600 °C (1 °C/min) in an inert atmosphere. The phenol–formaldehyde resin containing SE1010-silica was first heated to 200 °C under inert atmosphere for 30 min. Under these conditions further polymerization of the phenol–formaldehyde resin occurs, and the resulting silica becomes orange in color. Then, under a continuous flow of nitrogen, the temperature is increased to 600 °C over 1 h, held for 3 h, and again increased to 800 °C over 1 h.

Characterization Methods: TEM images were acquired on a Zeiss EM 912 Ω microscope at an acceleration voltage of 120 kV. Samples were ground in a ball mill and suspended in acetone. One droplet of the suspension was applied to a 400 mesh carbon-coated copper grid and left to dry in air. WAXS patterns were collected on an Enraf Nonius FR590 diffractometer. Ball-milled samples were irradiated for about 10 h. Nitrogen-sorption (T = –196 °C) data were obtained with a Micromeritics Tristar. Isotherms were evaluated with DFT [35]. Elemental analysis was carried out with a Vario EL from Elementar.

All Fourier transform IR (FTIR) spectra were recorded in direct (specular) transmission while the UV-vis/near-IR spectra were recorded in diffuse reflectance. Diffuse reflection spectroscopy measurements in the UV-vis/near-IR region were carried out on a Jasco VERY-570 spectrophotometer equipped with an integrating sphere. Spectra were recorded at RT from 200–900 nm with a scan-

ning speed of 100 nm min^{-1}, using $MgCO_3$ as a reference. IR spectra were recorded on a FTIR spectrophotometer BIORAD FTS 6000. The measurements were performed with normal incidence of light at wavelengths between 2.5 and 25 μm.

The measurements of the carbon-containing silicas in IR-reflectance mode were performed by Dr. V. Wittwer from the Fraunhofer-Institute for Solar Energy Systems in Freiburg.

Received: June 22, 2001
Final version: October 11, 2001

[1] C. G. Granqvist, *Materials Science for Solar Energy Conversion Systems*, Pergamon, Elmsford, NY **1991**.
[2] J. Salmi, J. P. Bonino, R. S. Bes, *J. Mater. Sci.* **2000**, *35*, 1347.
[3] E. Wackelgard, *J. Phys.: Condens. Matter* **1996**, *8*, 5125.
[4] P. J. Sebastian, J. Quintana, F. Avila, *Sol. Energy Mater. Sol. Cells* **1997**, *45*, 65.
[5] B. Carlsson, K. Moller, U. Frei, S. Brunold, M. Kohl, *Sol. Energy Mater. Sol. Cells* **2000**, *61*, 223.
[6] N. K. Raman, M. T. Anderson, C. J. Brinker, *Chem. Mater.* **1996**, *8*, 1682.
[7] J. S. Beck, J. C. Vartuli, *Curr. Opin. Solid State Mater. Sci.* **1996**, *1*, 76.
[8] T. J. Barton, L. M. Bull, W. G. Klemperer, D. A. Loy, B. McEnaney, M. Misono, P. A. Monson, G. Pez, G. W. Scherer, J. C. Vartuli, O. M. Yaghi, *Chem. Mater.* **1999**, *11*, 2633.
[9] N. Hüsing, U. Schubert, *Angew. Chem.* **1998**, *110*, 22.
[10] M. Adsten, R. Joerger, K. Jarrendahl, E. Wackelgard, *Sol. Energy* **2000**, *68*, 325.
[11] J. S. Liu, A. Ignatiev, *Sol. Energy Mater.* **1986**, *13*, 399.
[12] M. B. H. Mantelli, E. Bazzo, *J. Spacecr. Rockets* **2000**, *37*, 100.
[13] D. M. Mattox, R. R. Sowell, *J. Phys.* **1981**, *42*, 19.
[14] F. Milde, M. Dimer, C. Hecht, D. Schulze, P. Gantenbein, *Vacuum* **2000**, *59*, 825.
[15] K. Nagayama, A. S. Dimitrov, *ACS Symp. Ser.* **1996**, *648*, 468.
[16] G. Olalde, G. Flamant, D. Schwander, C. Combescure, *Proc. Soc. Photo-Opt. Instrum. Eng.* **1984**, *502*, 77.
[17] G. Olalde, G. Flamant, D. Schwander, C. Combescure, *Sol. Energy Mater.* **1985**, *12*, 461.
[18] Z. C. Orel, *Sol. Energy Mater. Sol. Cells* **1999**, *57*, 291.
[19] C. Riedel, *Tekstil* **1996**, *45*, 519.
[20] T. S. Sathiaraj, R. Thangaraj, O. P. Agnihotri, *Sol. Energy Mater.* **1989**, *18*, 343.
[21] S. Suzer, F. Kadirgan, H. M. Sohmen, *Sol. Energy Mater. Sol. Cells* **1999**, *56*, 183.
[22] T. Tesfamichael, E. Wackelgard, *Appl. Opt.* **1999**, *38*, 4189.
[23] E. Wackelgard, *Sol. Energy Mater. Sol. Cells* **1998**, *56*, 35.
[24] Q. C. Zhang, D. R. Mills, *J. Appl. Phys.* **1992**, *72*, 3013.
[25] S. Polarz, B. Smarsly, C. Göltner, M. Antonietti, *Adv. Mater.* **2000**, *12*, 1503.
[26] B. H. Han, S. Polarz, M. Antonietti, *Chem. Mater.* **2001**, *13*, 3915.
[27] T. Kyotani, *Carbon* **2000**, *38*, 269.
[28] S. Polarz, B. Smarsly, L. Bronstein, M. Antonietti, *Angew. Chem.* **2001**, *113*, 4549.
[29] C. G. Göltner, S. Henke, M. C. Weißenberger, M. Antonietti, *Angew. Chem.* **1998**, *110*, 633.
[30] K. W. Sing, *Adv. Colloid Interface Sci.* **1998**, *76–77*, 3.
[31] S. J. Gregg, K. S. W. Sing, *Adsorption, Surface Area and Porosity*, Vol. 2, 4th ed., Academic, New York **1982**.
[32] D. M. Mattox, *J. Vac. Sci. Technol.* **1975**, *12*, 1023.
[33] Z. C. Orel, M. K. Gunde, *Sol. Energy Mater. Sol. Cells* **2001**, *68*, 337.
[34] A. Schüler, J. Geng, P. Oelhafen, S. Brunold, P. Gantenbein, U. Frei, *Sol. Energy Mater. Sol. Cells* **2000**, *60*, 295.
[35] P. I. Ravikovitch, G. L. Haller, A. V. Neimark, *Adv. Colloid Interface Sci.* **1998**, *76–77*, 203.